1

Membrane Emulsification Process: Principle and Model

1.1 Introduction

Emulsions or particles prepared from emulsion with size-uniformity and size-controllability present distinctive advantages in industrial applications, such as microcapsules in drug delivery, particulate adjuvants for vaccination, and microspheres media in chromatographic separation and cell culture [1–4]. The early techniques of large-scale producing emulsion mostly depend on externally exerting strong dissipated energy into fluid mixtures, such as the rotor–stator, the high-pressure homogenizers, and the ultrasonic emulsification systems, in which the dissipated energy cannot be controlled homogeneously and the emulsion with broad size-distribution is often obtained. In recent decades, a great amount of work begins to explore the devices with milder and more controllable dissipating techniques to produce more uniform emulsion. Among the emerging devices, membrane emulsification technology (MET) has been addressed as a widely concerned group of uniform emulsification techniques, during which the to-be dispersed phase could grow into uniform droplets at uniform membrane pores with help of gentle and accurately controlled driving force [5]. Due to the controllability of droplet size by uniform membrane pore instead of the turbulent shearing flow, MET offers many advantages not only in narrow size distribution of droplets but also in lower energy requirement and suitability for emulsification of shear or temperature sensitive components.

According to different principles of emulsion preparation, the MET can be divided into two groups, the cross-flow membrane emulsification [6] and the premix membrane emulsification [7], also called as direct membrane emulsification and rapid membrane emulsification. The cross-flow MET is a process of two liquid phase flow. The to-be dispersed phase is pressed through the membrane's inner channel by pressure, generates the droplets at the membrane pores, and then the droplets until to a certain size are carried away by continuous phase fluid, as shown in Figure 1.1a. There are certain similarities existing between droplet breakup in premix and cross-flow emulsification depending upon the operating parameters. Comparatively, premix emulsification begins with a coarse emulsion, and then is extruded and homogenized through a porous membrane under a higher pressure to obtain fine emulsion, as shown in Figure 1.1b. Although the size of

Novel Membrane Emulsification: Principles, Preparation, Processes, and Bioapplications,
First Edition. Guanghui Ma.

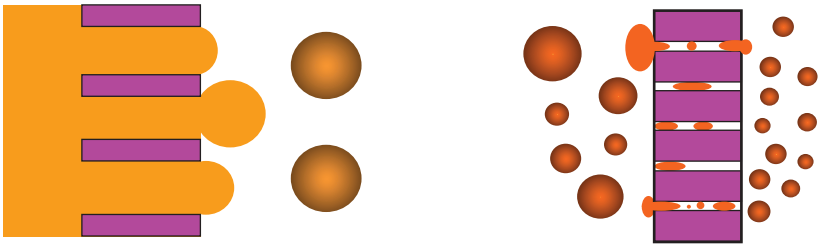

Figure 1.1 Two basic forms of membrane emulsification. (a) Cross-flow MET. (b) Premix MET.

the droplets is not as monodisperse as abovementioned cross-flow emulsification, premix emulsification is still an efficient route to produce emulsions with high dispersed-phase fraction.

The processing parameters of MET controlling emulsion droplet size and distribution have been extensively analyzed both experimentally and theoretically in these years [8–10]. A large number of empirical laws were discovered and a series of microscopic models were established by physics and mathematics language. Here, we would introduce the representative mechanisms of both cross-flow MET and premix MET and their developments over the years from macro to micro scales.

1.2 Cross-Flow Membrane Emulsification

During cross-flow MET, various parameters from different magnitudes would exert combined actions, including the interfacial surface property (diffusion, surface tension, and viscosity of two phases) and the macroscopic operation conditions (disperse phase velocity or pressure and continuous phase velocity) [6]. Generally, the droplet size was experimentally controlled primarily by the choice of membrane, the cross-flow velocity, and the transmembrane pressure. Typically, a factor of 2–6, depending on the properties of dispersed phase and continuous phase and even the structure of membrane is found between pore size and droplet size. Accordingly, the built numerical methodologies also aimed to describe the formation of droplet and predict the droplet size and the size distribution, such as the force and torque balances [11–13], surface free-energy minimization [14, 15], computation fluidic dynamics (CFD) [16], Lattice Boltzmann [17] and phase flow method [18], and so forth. These microscopic descriptions significantly facilitated the prediction of manufacturing throughput of emulsion and particle, optimization of MET operation, and design and scale-up of emulsion modules from laboratory to industrial production. The representative mechanisms and models involving cross-flow MET are intensively discussed as follows.

1.2.1 Mechanism of Droplet Formation

It has been observed that the uniformity of final emulsion mainly depends on the droplet formation behavior in membrane emulsification, except the cases of the

emulsion polydispersity caused by instability of the emulsion and wettability of the dispersed phase. Two mechanisms of droplet detachment behavior affecting size distribution were observed in cross-flow MET, i.e. the shear-induced droplet formation (SHE) and the spontaneous transformation-based (STB) droplet formation [19, 20]. The SHE mechanism describes the situation where droplet is detached by uneven shear force from cross-flow or rotary flow of continuous phase. The STB mechanism describes the situation where the droplet breaks off without any additional shearing and just by the variation of interfacial free energy. Droplet detachment driven by mechanism of STB at elongated outlet would result in more uniform emulsion than that driven by mechanism of SHE at circular outlet [21–23]. The Shirasu porous glass (SPG) membrane with a pore geometry composed of tortuous ellipsoidal cylinders has characteristics between circular and elongated outlets. Consequently, both mechanisms were observed via microscope visualization by tailoring the emulsification environments [19].

Here, we compared three typical emulsification environments, respectively, the anionic emulsifier (sodium dodecyl sulfate [SDS]), the nonionic stabilizer (polyvinyl alcohol [PVA]), and the cationic emulsifiers (acetyl trimethyl ammonium bromide [CTAB]) in water continuous phases. Meanwhile, the divinylbenzene was selected as the dispersed phase in O/W emulsion droplet. Figure 1.2 captures a typical spontaneous formation of droplet in continuous phase of 0.2% wt SDS solution. The droplet, respectively, experienced the growth, the staying and the detaching stages. Obviously, the staying stage lasts for the longest time and acted as the speed-limited step in droplet spontaneous formation and detachment.

This spontaneous behavior happened specifically at emulsifiers of nonionic PVA and anionic SDS at high concentrations of emulsifiers. As shown in Figure 1.3a, b, a droplet labeled with the fuzzy circles and arrows is moving out from the pore. Comparatively, the growing droplets tend to adhere to pores and refuse to detach in other emulsification environments, such as pure water and solutions, respectively, of CTAB $\geq$ 0.05% wt, low concentration of PVA $<$ 0.5% wt, and SDS $<$ 0.04% wt. These adhering droplets at adjacent pores tend to coalesce into larger droplets as shown in

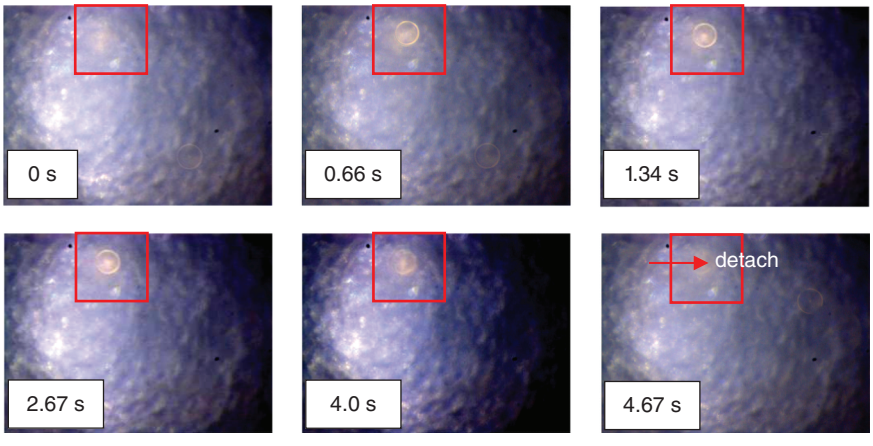

Figure 1.2 Growth of droplets on surface of SPG membrane.

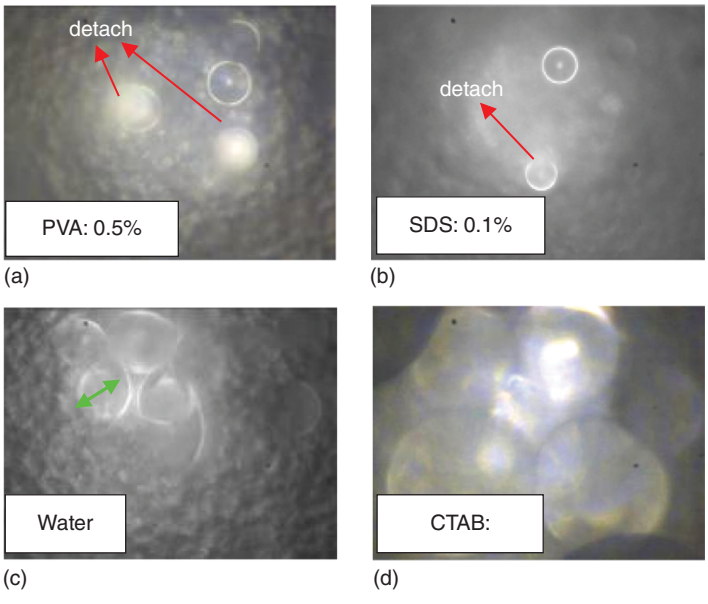

Figure 1.3 Droplets' spontaneous detaching and adhering behaviors.

Figure 1.3c, d, and have to be pulled out at a higher pressure or a strong shearing by continuous phase flow, and finally formed a polydispersed emulsion.

Because the interfacial tension between dispersed phase and continuous phase act as the major adhesion force on droplet, we further investigated the relationship between interfacial tension and droplet detachment behaviors. Figures 1.4 and 1.5 showed that the higher interfacial tension, such as in the case of PVA with concentration below 0.5%, would result in droplets adhesion and final polydispersed emulsion. However, if the interfacial tension could be decreased effectively to the lowest, such as in solution of SDS above 0.2%, the droplet would demonstrate an obvious spontaneous detachment and the uniform emulsion would form finally as shown in Figures 1.6 and 1.7. It can be speculated that the droplet's spontaneous detachments could effectively avoid the coalescence between droplets and nonuniform shearing

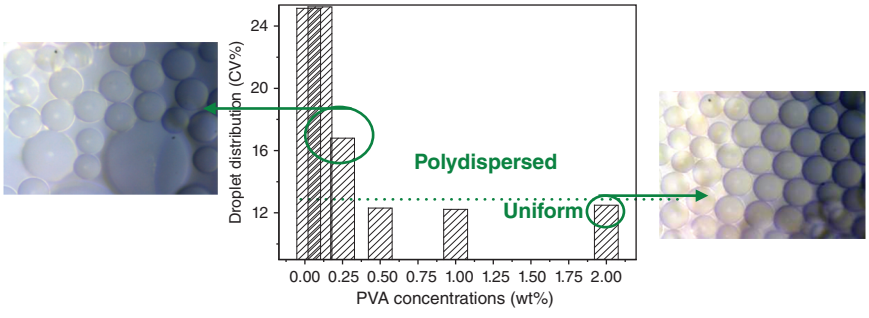

Figure 1.4 Droplets distributions at different PVA concentrations.

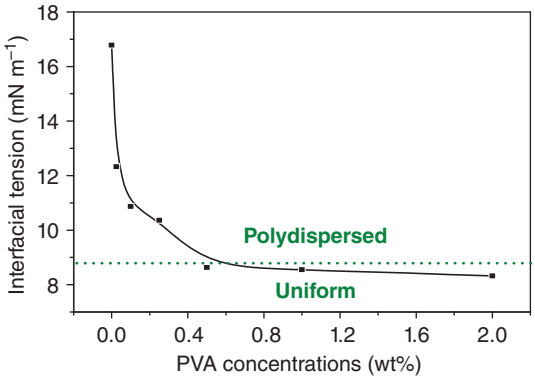

Figure 1.5 Interfacial tension of oil–water phase at different PVA concentrations.

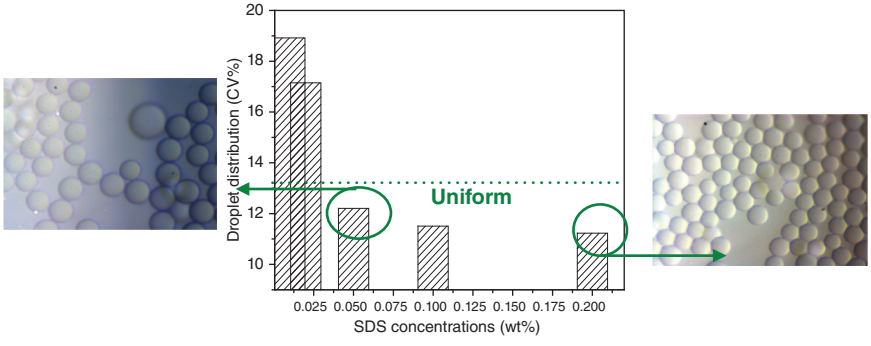

Figure 1.6 Droplets distributions at different SDS concentrations.

Figure 1.7 Droplets distributions at different SDS concentrations.

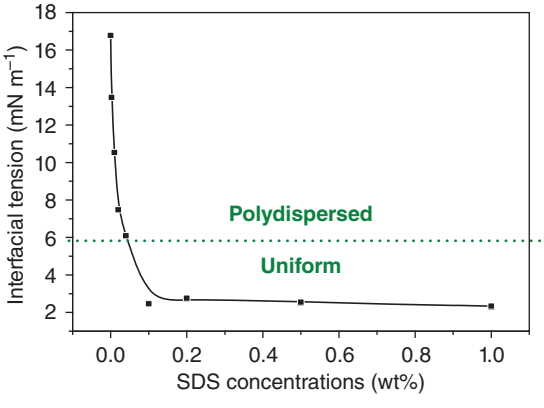

field from continuous phase flow, and finally form uniform emulsion as shown in Figures 1.6 and 1.7. Comparatively, SDS showed stronger ability to decrease interfacial tension and presented more significant tendency of spontaneous detachment, and could prepare more uniform droplets. It confirmed again that the spontaneous formation behavior of droplets would facilitate uniform emulsion formation.

1.2.2 Force Balance Model

The force balance model are the most universal explanation for various experimental phenomena and laws during membrane emulsification [12, 24]. The description of individual droplet formation and detachment by forces is very intuitive and easily understood. As shown in Figure 1.8, it focuses on analysis of microscopic forces on droplet at moment of droplet gushing out from membrane pores, including the shear force F_{cf}, the buoyancy force F_B, the interfacial tension force F_γ, and the static pressure difference force F_{sp}.

Specifically, the interfacial tension force,

$$F_\gamma = \pi d_p \gamma(t) \tag{1.1}$$

represents the effects of dispersed-phase adhesion on pore opening as the retaining force for adhesion.

The static pressure difference force F_{sp} is the force caused by pressure difference between the dispersed phase and the continuous phase at membrane surface. In quasi-static state, it is described as as follows:

$$F_{sp} = (P_i - P_o)A_p = \Delta P_\gamma A_p = \pi\gamma(t)d_p^2/d_{dr} \tag{1.2}$$

where A_p is the cross-sectional area of the droplet neck at pore and here approximately assumed as area of pore, and d_{dr} is the dynamic droplet diameter, which is increasing until droplet detaches from pore.

The cross-flow drag force, F_{cf}, is created by the continuous phase flowing past the droplet parallel to membrane surface [25]. According to Stokes' equation in a simple shear flow and assuming that the droplets are formed in laminar sublayer, it is described as as follows:

$$F_{cf} = 3\pi u_c d_{dr} \mu_c \tag{1.3}$$

The dynamic lift force, F_{dl}, results from the asymmetric velocity profile of the continuous phase near droplet and is defined as follows:

$$F_{\mathrm{dl}} = 0.761 {\tau_w}^{1.5} {d_{dr}}^3 {\rho_c}^{0.5}/\mu_c \tag{1.4}$$

in which, shearing force τ_w is controlled by the continuous phase velocity u_c [22] and is deduced based on the definition of Fanning friction factor as given below:

$$\tau_w = f\frac{\rho_c u_c^2}{2} \tag{1.5}$$

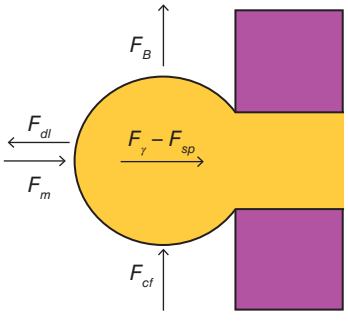

Figure 1.8 Force analysis of droplets on outlet of membrane pore.

where ρ_c is the density of continuous phase, u_c is the flow velocity of continuous phase, and f is a dimensionless factor defined by the Reynolds number Re as follows:

$$f = \begin{cases} 16/\mathrm{Re} & \mathrm{Re} < 2000 \\ 0.00140 + 0.125/\mathrm{Re}^{0.32} & 2 \times 10^3 < \mathrm{Re} < 3 \times 10^6 \end{cases} \tag{1.6}$$

where $\mathrm{Re} = \rho_c u_c D/\mu_c$, D is the inner diameter of the cross-flow channel (membrane channel), and μ_c is the viscosity of continuous phase.

If the density of dispersed phase cannot be neglected, the buoyancy force F_B of a droplet with volume V_d should be amended as the resultant force F_{BG} of buoyancy and gravity F_G, and described as the density difference between two phases.

$$F_{BG} = F_B - F_G = (\rho_c - \rho_d) g V_d \tag{1.7}$$

The linear momentum force F_m is caused by flow movement of a mass of dispersed phase out from the pore outlet.

$$F_m = \int_{A_p} \rho_d {v_d}^2 dA = \frac{\pi}{4} \rho_d u_d^2 d_p^2 \tag{1.8}$$

Among these forces, F_γ is the holding force to make droplets adhere at membrane pore outlet, while F_{dl}, F_{BG}, F_m, and F_{cf} are the detaching forces to drive droplets away from pores, and the inertia forces F_m and buoyancy forces F_{BG} can be neglected when they are approximately from six to eight orders of magnitude smaller than other forces after calculation. If the total adhesion forces are greater than the detaching force, the droplet would continue to grow on outlet of membrane pore. If the adhesion forces are less than the detaching forces, the balance of forces on the droplet is lost, and the droplet begins to deform, elongate, form a neck, detach from the membrane pore, and finally enter the continuous phase. The contributions of various forces depended on droplet size. For smaller micron-size pores, the inertial and buoyancy forces are much smaller than the viscous drag force and surface tension, respectively, and thus can be ignored in balance model; otherwise, they will play vital role for large droplets with hundreds of microns.

The prototype of force balance model was first put forward by Peng and Williams in 1998 [26]. They predicted the size of droplet generated from the capillary with inner diameter of 45 microns and considered that the droplet surface was mainly affected by forces, including the flow drag force (F_{cf}, generated by the continuous phase shearing action parallel to membrane surface), the buoyancy force (F_B, generated by the density difference between two phases), and F_γ (represents the force generated by the interfacial tension). Three forces get balanced as $F_{cf} + F_B = F_\gamma$. Schroder and Wang supplemented this microscopic forces model with more accurate descriptions, including the static pressure difference force (F_{SP}, generated from the pressure difference between the continuous phase inside and outside the droplet), the dynamic lift force (F_{dl}, generated from the asymmetric velocity distribution profile of continuous phase near the droplet), and the inertial force (F_m, related to the momentum of fluid movement flowing out of the membrane orifice) [27, 28]. Further, Xu et al. introduced variables of continuous phase flow velocity in force balance model and attempted to predict the change rule of

emulsion droplet size under different continuous phase velocities [29]. They found that the force balance model agreed well with the experimental data. The droplet size and droplet formation time decreased with increase of continuous phase flow rate. Since their emulsification experiment was completed in continuous phase without emulsifier and the droplet size was obtained from microscope observation at membrane pore, the equipment and environment of their prediction were still quite different from the actual membrane emulsification. In addition, the dynamic oil–water interfacial tension of droplet surfaces and the influence of operating conditions of dispersed phase on emulsification process were not considered in both of their experiments and model.

Later, G. De Luca et al. introduced more variables, including the dispersed phase transmembrane pressure and the dynamic interfacial tension into abovementioned force balance model. The coupling effect of these variables on the droplet size was investigated [11]. They found that if droplet formed earlier than the interfacial tension arriving at equilibrium, the droplet size was directly proportional to the transmembrane pressure. Conversely, it was not related to the transmembrane pressure. They developed a modified balance model from another perspective of contact line [30]. It is assumed that the film surface exists as long as the force arrives in balance near the contact line; the droplet will adhere to the edge of membrane pore in an inclined position and deform until it finally detach from pore. In the force balance formula based on the contact line, all the forward contact angles, backward contact angles, and the minimum and maximum volume of droplet growth could be calculated (Figure 1.9). The validation of this model is completed under different conditions, including continuous phase velocity, membrane pore size, and interfacial tension. The linear relationship between droplet size and membrane pore size and the change of interfacial tension during droplet formation are all predicted.

1.2.3 Torque Balance Model

Above mentioned force balance models define the generated droplet as a point and the droplet will peel off immediately after two groups forces arriving balance,

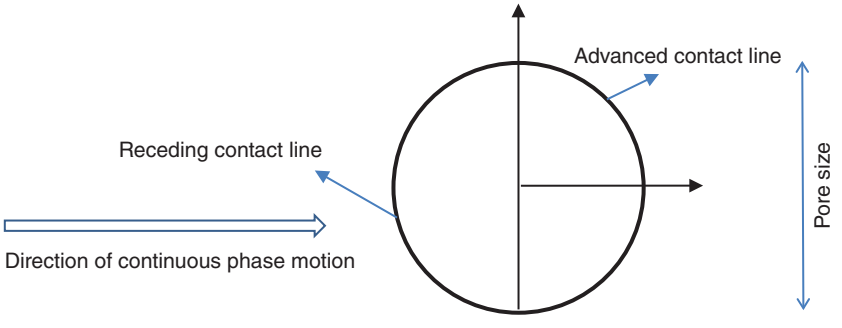

Figure 1.9 Schematic representation of contact line (top view) for a circular shape forming the droplet basis.

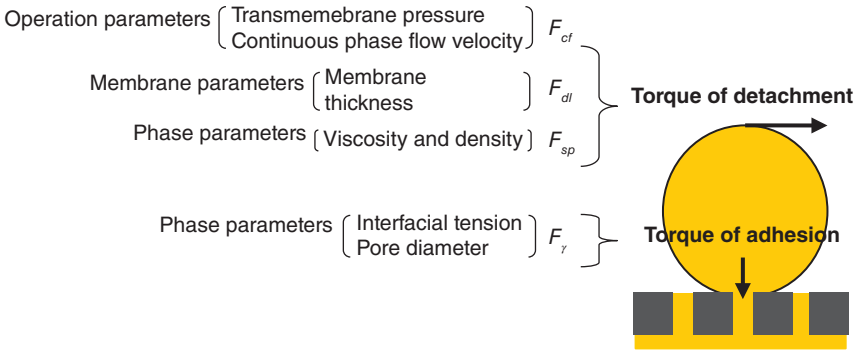

Figure 1.10 Torques and forces on droplet at membrane outlet. Source: Hao et al. [13]/with permission of American Chemical Society.

while the torque model regards the droplet as a sphere, and the droplet will rotate and escape from membrane pore until torques on droplet surface getting balance. The difference between two models lies in their comprehension of emulsion droplet. Torque model provides more accurate description and couples more parameters than force balance model in case the diameter of large droplet during its detachment cannot be ignored. According to the framework of torques on a droplet as shown in Figure 1.10, the torques of adhesion and the torques of detachment can be grouped. It indicates that the rules of torques manipulate the droplet behaviors and can be examined by coupling operation parameters, membrane parameters, and physiochemistry properties of two phases. Therefore, we build a multivariable torque model to obtain the influences of different parameters on droplet detachment mechanism. Before multivariables torque model, two sets of relationships associating the dispersed phase parameters and the continuous phase parameters should be firstly constructed given in the following sections.

1.2.3.1 Associating the Dispersed-Phase Parameters

During droplet growing up at membrane pore, the dispersed phase flow rate Q_{dr} through the membrane pores may be assumed based on Darcy law and Hagen–Poiseuille equation as follows [11]:

$$Q_{dr} = \pi d_p^4 P_{ef}/(128\xi\mu_d L) \tag{1.9}$$

where d_p is membrane pore and here used 5.2 μm, ξ is the pore tortuosity and here approximatively used as 2.1, which was measured and calculated with hydraulic membrane resistance by Vladisavljevic [8], μ_d is the viscosity of dispersed phase, and L is the membrane thickness. P_{ef} is the effective transmembrane pressure to control the dispersed phase and defined as the difference of two pressures,

$$P_{ef} = P_{trm} - P_{\gamma} = P_{trm} - 4\gamma(t)/d_{dr} \tag{1.10}$$

where P_{trm} is the transmembrane pressure applied in emulsification between each side of membrane, and P_{γ} is the capillary pressure.

The dynamic droplet volume V_d can be related to dispersed-phase flow rate Q_{dr} by following continuity equation of dispersed phase, as given below:

$$\frac{dV_{dr}}{dt} = Q_{dr}[h(t), \gamma(t)] \tag{1.11}$$

and the volume of droplet as a spherical cap can be calculated with the growing height $h(t)$ of droplet at membrane pore as follows:

$$V_{dr}[h(t)] = \frac{1}{6}\pi h(t)\left(\frac{3}{4}d_p^2 + h(t)^2\right) \tag{1.12}$$

The dynamic height of droplet $h\ (t)$ can thus be deducted by (1.11), (1.12), and (1.9),

$$\begin{aligned}\frac{dh}{dt} &= \left(\frac{dV_d}{dt}\right) \Big/ \left(\frac{dV_d}{dh}\right) = \left(\frac{dV_d}{dt}\right) \Big/ \left[8\pi\left(d_p^2 + 4h^2\right)\right] \\ &= \frac{d_p^4}{16\mu_d \xi L}\left[\frac{P_{tm}}{d_p^4 + 4h^2} - \frac{16\gamma(t)h}{\left(d_p^2 + 4h^2\right)^2}\right]\end{aligned} \tag{1.13}$$

Droplet diameter $d_{dr}\ (t)$ can also be described by height of droplet $h\ (t)$,

$$\frac{d_{dr}}{2} = \frac{\left(\frac{d_p}{2}\right)^2 + h^2}{2h} \tag{1.14}$$

So, the droplet growth $d_{dr}\ (t)$ can be deducted from Eqs. (1.13) and (1.14):

$$\frac{d(d_{dr})}{dt} = \frac{d(d_{dr})}{dh}\frac{dh}{dt} = \left(1 - \frac{1}{4}\frac{d_p^2}{h^2}\right)\frac{d_p^4}{16\mu_d \xi L}\left[\frac{P_{tm}}{d_p^4 + 4h^2} - \frac{16\gamma(t)h}{\left(d_p^2 + 4h^2\right)^2}\right] \tag{1.15}$$

The initial conditions for Eqs. (1.14) and (1.15) are established according to Laplace equation with initial interfacial tension and critical pressure,

$$d_{dr}(0) = 4\gamma(0)/P_\gamma{}^0 \text{ and } P_\gamma^0 = 16\gamma(0)h(0)/\left[d_p^2 + 4h(0)^2\right]$$

where $h\ (0)$ is also determined by Eq. (1.14).

1.2.3.2 Associating the Continuous Phase Parameters

The shear force τ_w is the function of the continuous phase velocity u_c [29],

$$\tau_w = f\frac{\rho_c u_c^2}{2} \tag{1.16}$$

where ρ_c is the density of continuous phase, u_c is the flow velocity of continuous phase, and f is a dimensionless factor defined by the Reynolds number Re as Equ. 1.6.

1.2.3.3 Torque Balance Model Associating Operation Parameters

Among all the aforementioned forces on droplet, F_γ is the holding force, while F_p, $F_{\gamma m}$, F_{BG}, F_m, and F_τ are detaching forces. The inertia force F_m and the buoyancy force F_{BG}, can be neglected after calculation considering that they are approximately

from six to eight orders of magnitude smaller than other forces. So, all the torques on droplet can be grouped as follows:
the torque of adhesion,

$$T_{\text{adhesion}} = F_{\gamma}\frac{d_p}{2} = T_{\text{adhesion}}[\gamma(t), d_p] \tag{1.17}$$

and the torque of detachment,

$$T_{\text{detach}} = F_{sp} + F_{dl}\frac{d_p}{2} + F_{cf}h = T_{\text{detach}}[\gamma(t), d_p, h(t), d_{dr}(t), \tau_w(u_c), \rho_c, \mu_c] \tag{1.18}$$

If the adhesion torque (or interfacial tension) was very large at the balance point of two torques, $T_{\text{adhesion}} = T_{\text{detach}}$, the droplet would be difficult to break off and a larger detachment torque (shearing stress) was needed and tend to be dragged by the SHE mechanism instead of the STB mechanism [31]. Therefore, we put forward that the torques at the balance point could act as a comparison criterion to estimate the transformation of the droplet detachment mechanism and further the emulsion uniformity, inspired by that droplet spontaneous formation (STB mechanism) is one of the most important mechanisms to form a uniform emulsion [13]. Since the torque model is constructed by coupling the operating parameters, the membrane parameters, and the physiochemistry properties of the two phases, the disturbances of these parameters on torques can be calculated to predict their influences on emulsion uniformity. Based on above mechanisms and parameters associated in torque models, we further explored the rules of controlling emulsion uniformity by experiment and theoretical approaches [13].

1.2.3.4 Evaluation of Controlling Factors on Droplets Uniformity by Torque Balance Model

Accordingly, the influence of operation conditions, the physical properties of two phases, and the membrane parameters on droplet formation and emulsion uniformity were systemically investigated by evaluating the variable force torques in droplet formation process. The experiment phenomena showed a good coincidence with model prediction. The conditions facilitating the production of uniform droplets were summarized as: (i) the high enough interfacial tension between the dispersed phase and the continuous phase, (ii) low cross-flow velocity of the continuous phase, (iii) low transmembrane pressure, (iv) high viscosity of the dispersed phase, and (v) an emulsifier with great ability and rapid rate to decrease interfacial tension.

1.2.3.4.1 Influence of Continuous Phase Flow on Emulsion Uniformity

The flow rate of continuous phase is a fundamental process parameter to determine membrane emulsification efficiency because the wall shear stress by continuous phase is the major force to drive the droplets detaching from membrane pore. The effects of different continuous phase flow rates on emulsion uniformity were investigated by O/W emulsification experiments. Figure 1.11 shows that the distribution of droplet size (CV%) can keep narrow at a wide range of the continuous phase flow rate from 0.188 to 1.85 m s^{-1}. However, with further increase of continuous phase

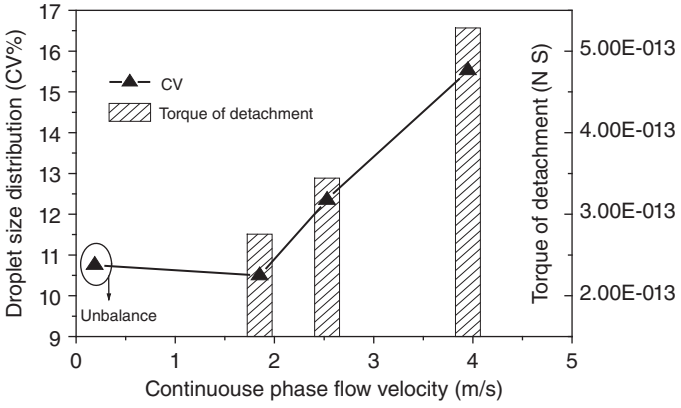

Figure 1.11 Influence of continuous phase flow velocity on droplet size distribution by experiment and detachment torques analysis. Source: Hao et al. [13]/with permission of American Chemical Society.

flow from 1.85 to 3.95 m s^{-1}, the droplet size distribution changed to broad quickly. Figure 1.11 also compared the relationship between droplet size distribution and the related predicted torques at balance. A general tendency was found that the emulsion uniformity (CV%) was spoiled at large detachment torque (at balance point) with continuous flow rate increases.

Figure 1.12 describes the development of two types of torques calculated, the adhesion one and the detachment one. Because the adhesion torque is a function of dynamic interfacial tension, the curve of adhesion torque presents the same change with the dynamic interfacial tension, which decreases sharply at beginning and then comes to equilibrium. The curve of detachment torque also presents a decreasing trend with droplet formation time. Two types of torques get balanced at intersection point of curves. The balance point of torques continues to rise up with continuous

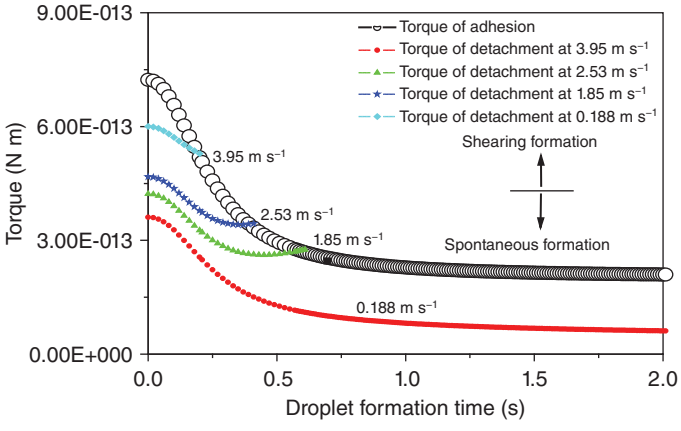

Figure 1.12 The development of torques on global droplet at different continuous phase flow velocity. Source: Hao et al. [13]/with permission of American Chemical Society.

phase flow increasing from 1.85 to 3.95 m s^{-1}, indicating that the droplet detachment tended to be controlled by mechanism of shearing formation and the uniformity of emulsion became worse with increase of continuous phase flow rate. Consequently, based on the different balance points of torques, the droplet detachment behavior can be divided into three zones. (i) At a low continuous phase flow velocity of 0.188 m s^{-1}, the torque of detachment is far below the torque of adhesion and never gets balance. It is speculated that the detachment of droplets is driven by mechanism of STB in this zone. (ii) The torque of detachment could reach to balance point with the torque of adhesion at small level. In this zone, both mechanisms of STB and SHE take effect on droplet, which manipulate the droplet continuously growing up and experiencing a distorting and necking stage before totally breaking off. (iii) The torque of detachment arrived at the balance point with the torque of adhesion at large level. In this zone, the mechanism of SHE is dominant for droplet detachment, which drags the droplets immediately away from the membrane pore and the necking stage can be neglected. Experiments showed that if the operating conditions were controlled in the zones (i) and (ii), the relatively uniform emulsion would be produced.

1.2.3.4.2 Influence of Transmembrane Pressure on Emulsion Uniformity

Another parameter strongly affecting the droplet size distribution is the transmembrane pressure, which controls the flux rate of dispersed phase across the membrane channel and thus the development of detachment torque. Figure 1.13 shows that the detachment torque curves rose up with transmembrane pressures increasing. They intersected with adhesion torque curve at the earlier and larger balance point, indicating that the high transmembrane pressure would lead to the detachment mechanism of SHE and the polydisperse emulsion. This speculation was demonstrated by change in droplets' size distribution under different emulsification pressure observed in Figure 1.14. When the dispersed-phase transmembrane pressure increased from critical pressure 8–14 kPa, the CV value increased slightly

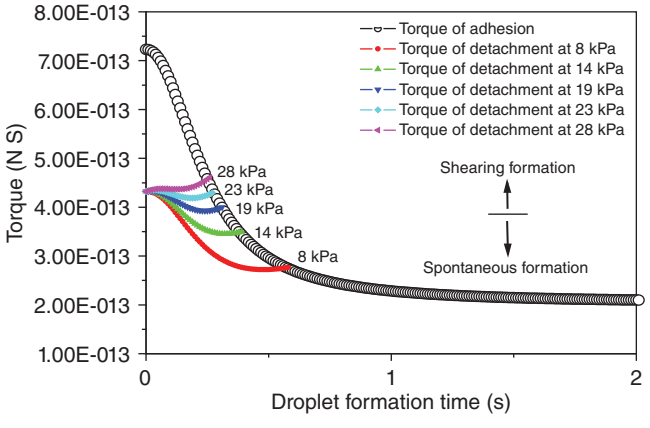

Figure 1.13 The development of torques on global droplet at different transmembrane pressure. Source: Hao et al. [13]/with permission of American Chemical Society.

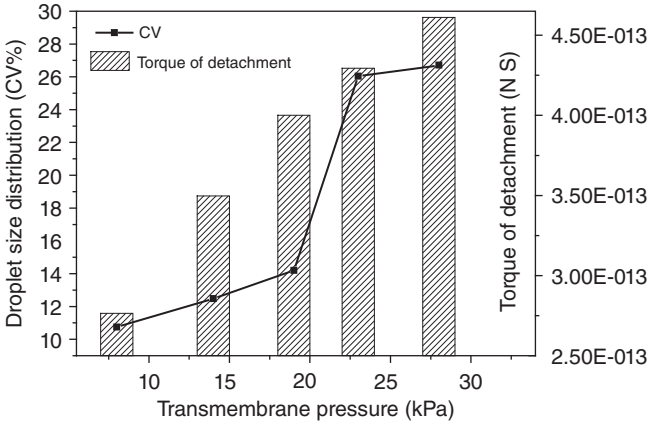

Figure 1.14 Influence of transmembrane pressure on droplet size distribution by experiment and detachment torques prediction. Source: Hao et al. [13]/with permission of American Chemical Society.

from 11% to 14%, and then rise above 26% when transmembrane pressure was increased to 28 kPa.

1.2.3.4.3 Influence of Viscosity of Dispersed Phase on Emulsion Uniformity

To evaluate the influence of viscosity of dispersed phase, two systems of dispersed phase, divinylbenzene and soybean oil, were compared since they have different viscosity but similar dynamic interfacial tension and density. The calculation of torques in Figure 1.15 shows that the torques of dispersed phase with high viscosity would get to balance later, implying that the droplet would easily break from the pores and tend to the spontaneous detachment mechanism and uniform emulsion. Abovementioned speculations were observed by the emulsification experiments in Figure 1.16,

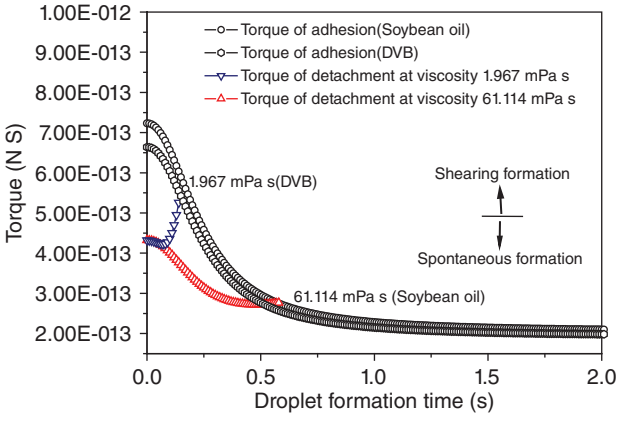

Figure 1.15 The development of torques on global droplet at different viscosity of dispersed phase. Source: Hao et al. [13]/with permission of American Chemical Society.

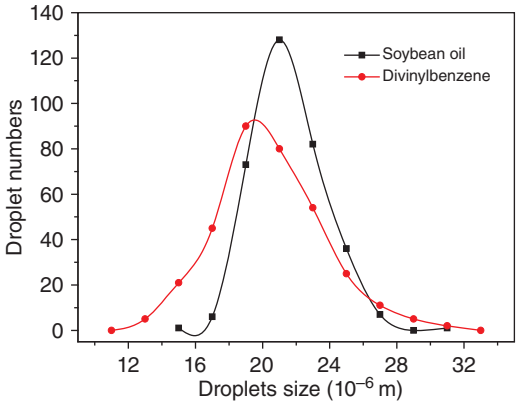

Figure 1.16 Droplet size distribution of dispersed phase with different viscosity. Source: Hao et al. [13]/with permission of American Chemical Society.

where the droplet of soybean oil with high viscosity had a narrower size distribution than that of divinylbenzene with low viscosity.

1.2.3.4.4 Influence of Emulsifiers or Stabilizer on Emulsion Uniformity

The dispersants (such as emulsifiers and stabilizer) dissolved in continuous phase also play critical roles on membrane emulsification [31]. They not only decrease the interfacial tension between dispersed phase and continuous phase by adsorption at newly formed interface of droplet and thus depress the critical transmembrane pressure in emulsification operation but also can restrain the coalescence and aggregation between emulsion droplets. Three typical dispersants, SDS, Tween 20, and PVA often used in membrane emulsification, were evaluated here by torque balance model [28, 31, 32]. SDS with the highest surface activity could rapidly reduce the interfacial tension of dispersed phase to the lowest equilibrium value. Consequently, because the interfacial tension force is a major force holding droplet at membrane pore, SDS with strong ability to lower the interfacial tension would provide the smallest adhesion torque for droplet and a smaller detachment torque for balance (Figure 1.17). It facilitates the droplet easily detaching from the membrane pore at the spontaneous droplet formation (STB mechanism) mode and the uniform emulsion was finally produced (Figure 1.18). Comparatively, the stabilizer PVA cannot effectively reduce the interfacial tension as SDS and Tween 20, and contribute to the larger adhesion torque on droplet in MET (Figure 1.17). It finally drives the droplet detachment with the shearing (SHE) behavior and results in the polydisperse emulsion (Figure 1.18), although it presents the best stabilizing ability for droplets in suspension [32].

Calculation of torque curves with different dispersed phases shows that above tendency also depended on the initial interfacial tension of dispersed phase. When liquid paraffin was used as the dispersed phase, its initial interfacial tension was very large as 46 mN m. It led to a significant raise of adhesion torque curve and larger balance point of torques than the soybean oil (Figure 1.19), which consequently formed the polydispersed emulsion in experiment (Figure 1.20). Comparatively, the soybean oil with low interfacial tension of 17 mN m was calculated to arrive at the lower

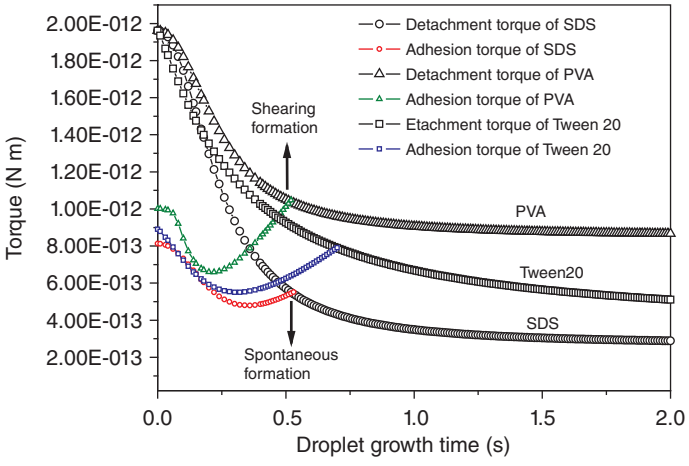

Figure 1.17 The development of torques on global droplet of paraffin by using SDS, Tween 20, and PVA as emulsifiers and stabilizers. Source: Hao et al. [13]/with permission of American Chemical Society.

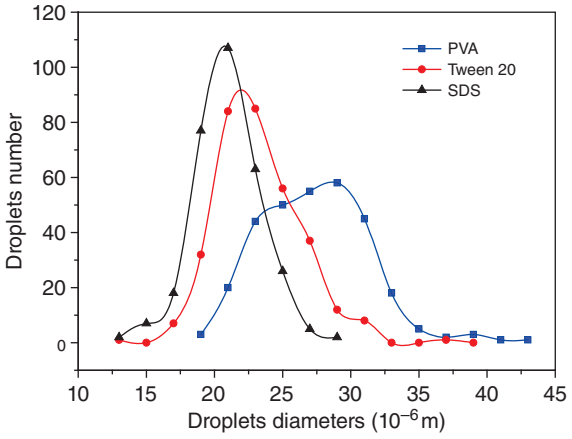

Figure 1.18 The droplet size distribution of paraffin by using SDS, Tween 20, and PVA as emulsifiers and stabilizers [13].

balance point with a spontaneous formation mode and coincide with the uniform emulsion formation in experiment (Figure 1.20).

1.2.4 Computational Fluid Dynamics

Although force and torque models represented sufficient comprehensiveness in incorporating various controlling parameters in membrane emulsification, their macroscopic cognization on emulsification was still limited and their prediction accuracy was much weaker. The microscope models established by CFD provide more dynamic behavior of droplets and are not limited to the droplet size. The basic procedure of CFD in simulation of droplet flow at pores could be described as follows. Firstly, the discrete distribution of flow field around droplet was obtained in continuous region by numerically solving the differential equation controlling

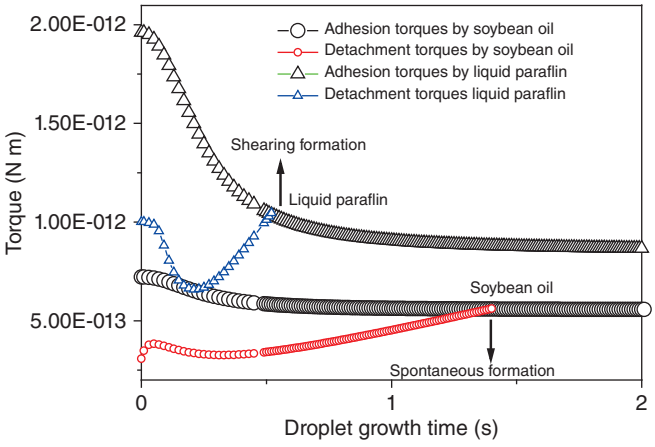

Figure 1.19 The development of torques on global droplet by different dispersed phase by using PVA as a stabilizer. Source: Hao et al. [13]/with permission of American Chemical Society.

Figure 1.20 The droplet size distribution of different dispersed phase with PVA as a stabilizer. Source: Hao et al. [13]/with permission of American Chemical Society.

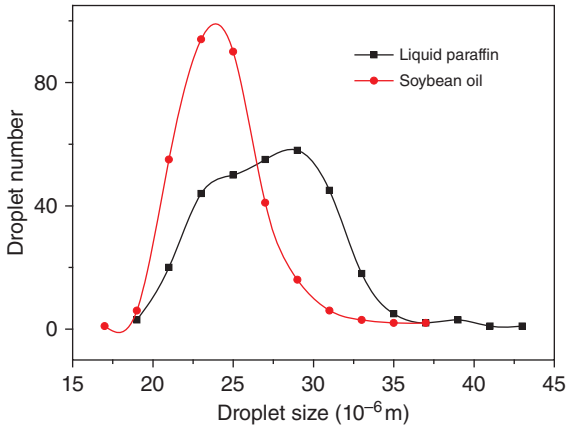

the fluid flow. Then the fluid mechanics of droplet movement was approximately simulated, and meanwhile, the visualization of these calculations was realized. By commercial software CFX4.2 developed based on CFD, A. J. Abrahamse et al. described the shape change of droplet at the membrane pore [33]. The simulation environment and boundary conditions were defined as the three-dimensional multiphase Reynolds flow, 5 μm cylindrical hole, rectangular continuous phase flow channel, 0.5 m s^{-1} continuous phase velocity, and 1.3 MPa driving pressure of dispersed phase. Accordingly, a critical distance between pores was identified as the distance between pores must be less than ten times of pore aperture in x-axis direction and seven times in *y*-axis direction, otherwise the droplets at adjacent pores would aggregate with each other. So according to the staggered arrangement of pores, the maximum void fraction without coalescence could be determined as 1.5%. Besides this, CFD also presents a complete visualization of microscale

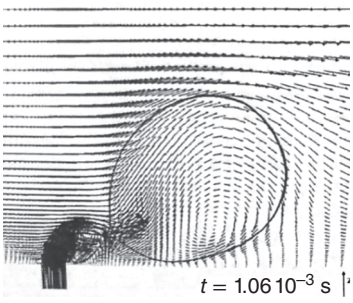

Figure 1.21 The microdynamic behavior of droplet simulated by CFD. Source: Abrahamse et al. [33]/John Wiley & Sons.

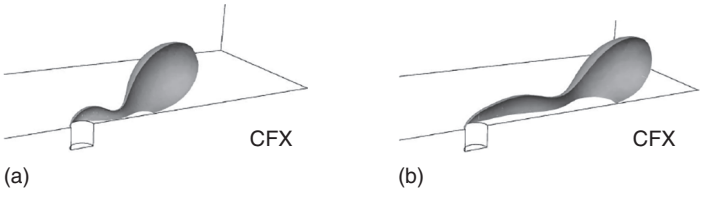

Figure 1.22 Droplet deformation process simulated by CFX: (a) the wall contact angle of 30° and (b) the wall contact angle of 60°. Source: Gijsbertsen Abrahamse et al. [2]/with permission of Elsevier.

dynamic growth of droplets. As shown in Figure 1.21, the droplet firstly formed a long neck during detachment, then the long neck is gradually torn to help the droplet completely detach, and finally the torn neck will stay at the membrane pore to form another new small droplet.

The effect of wall contact angle between droplet and pore surface on formation and shape change of droplet was interpreted by Abrahamse et al. with CFD [2, 34]. Their discovery is consistent with the microscopic observation of membrane emulsification [35]. As shown in Figure 1.22, the large wall contact angle would result in spreading of droplet and polydisperse emulsions by extending the contact edge of droplet on pore solid surface, prolonging their retention and spreading into large droplet. Consequently, a critical value of wall contact angle to avoid droplet spreading could be identified as 60°.

The pore shapes, such as circular and elliptical outlets of pores, were also found to influence the droplet formation by Kobayshi et al. with CFD [16]. As shown in Figure 1.23, the droplet at membrane pore would experience a gradual process of droplet necking, neck elongating, neck fracturing, and droplet detaching. During deformation of droplet, the droplet necking on circular pore will form a complete contact line to cover the whole pore outlet, while the droplet necking on elliptical pore will be permeated by the continuous phase flow into the pore channel and then lead to a rapid increase of fluid pressure and velocity around the necking, the instantaneous cut of neck, and finally the spontaneous formation of smaller droplet.

The advantage of CFD in analysis of membrane emulsification is that it realized both accurate calculation and visualization of microscopic flow field around and inside droplet. It allows for the consideration of more complexities, such as the active pore distribution and the droplets interaction, than the simplified force and torque

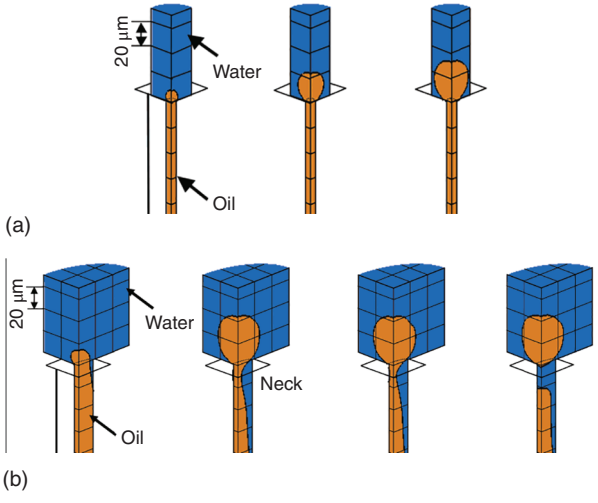

Figure 1.23 Deformation of droplets on surface of different membrane pores: (a) circular pore and (b) elliptical pore. Source: Kobayshi et al. [16]/with permission of American Chemical Society.

balance models. However, CFD still features the inherent limitations, e.g. the reliability relying on the clear definition of sufficient physics data and requirement of commercial software.

1.2.5 Models by Surface Evolver Tool

Surface Evolver tool is a set of interactive finite element software packages developed by the National Center for science and geometry calculation and visualization technology of University of Minnesota. It described the static equilibrium state of liquid and the interfaces shaped by surface potential energy and other energies. Rayner et al. investigated the droplet formation mechanism from the point of view of Gibbs free energy by Surface Evolver (Figure 1.24) [14]. They tracked the droplet shape as it grows and identified the point of instability due to free energy, and thus predict the droplet size. They also compared the prediction with the emulsification experiment with membrane of oblong-shaped pores by Kobayashi [36]. The models were inputted with the pore geometry, oil/aqueous phase interfacial tension, contact

Figure 1.24 Shape of droplets simulated by Surface Evolver. Source: Rayner et al. [14]/with permission of Elsevier.

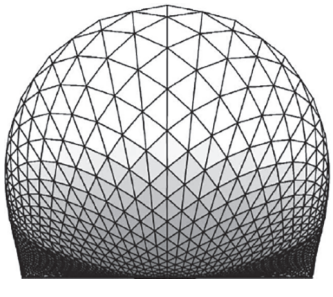

angle, the geometric definition of the surface as vertices (points), edges (vectors), facets (triangles), bodies (groups of oriented facets), constraints, methods, and the boundary conditions to calculate the various energies. The model reasonably predicted the droplet sizes under quiescent conditions with the average error of 8% from the experimental data. They further considered the influence of dynamic interfacial tension of the emulsifier and flow rate of dispersed phase on the shape of the droplet [15]. They found that both the droplet size and its prediction error would increase with the flow rate of the dispersed phase increasing since the emulsifier cannot be replenished to the newly grown interface in time and the interfacial tension during droplet detaching interface was very large. Surface Evolver approach accounted for the issues about the nonspherical shape of membrane pore, but was limited in the prediction inaccuracy by membrane wetting and not widely popularized as other models due to its complexity and time-consuming software processing.

1.2.6 Models by Lattice Boltzmann Method

Unlike CFD simulating the continuous fluid, Lattice Boltzmann method (LBM) is based on the hypothetical particles (packages of fluid) that move and collide in a lattice according to the kinetic gas theory. It thus can incorporate both physical and thermodynamic components such as surfactants and polymers in membrane emulsification. By LBM, Sandra van der Graaf et al., describe the fluid movement of droplet interface in a T-shaped microchannel emulsification, droplet deformation between two shearing plates, and a sessile drop on a plate with different wetting conditions (Figure 1.25) [17]. They found that the capillary (Ca) number contributes to the growth and detachment stage of droplet. In the case of a higher Ca and a higher dispersed-phase flow rate, the necking volume of droplet will contribute considerably to the final droplet volume, and otherwise the necking volume during detachment stages can be negligible.

As a whole, aforementioned models mostly focused on the moment of single droplet formation and detachment at membrane pore. They realized the prediction of droplet size with different precision preferentially on the physical properties of forces or energy. Besides these, some models from another perspective provided insight into problems of interaction, coalescence, and uniformity between multiple droplets [13, 33, 37–40]. Some others aimed at the flow behavior by introducing the dimensionless groups' number, such as Re, We, and Ca, to describe droplet formation from individual droplet to multiple droplets [41–43]. Considering the

Figure 1.25 Movement of droplets simulated by Lattice Boltzmann method. Source: Van der Graaf et al. [17]/American Chemical Society.

calculation power and time, hardware and software availability, the utilization of them always compromises between accuracy and requirement. Nonetheless, all of these models enriched the microscope information beyond the experiment's visualization from different scales and satisfied the various requirements for membrane emulsification design and optimization.

1.3 Premix Membrane Emulsification

The simplicity of premix emulsification (also named as rapid membrane emulsification), as shown in Figure 1.1b, provided a promising option for large-scale membrane production of emulsions, although many aspects have not been well understood. As mentioned, premix emulsification begins with a coarse emulsion, and then this emulsion is extruded through a membrane under pressure to obtain a fine emulsion. The resulting emulsion is mostly characterized by the productivity and related to the transmembrane flux. The transmembrane flux (J) is defined as follows:

$$J = \frac{Q}{A}$$

where Q is the volumetric flow rate, and A is the cross-sectional area of the membrane.

The actual velocity in pores, $\sigma_{w,p}$, is a function of flux and porosity of membrane as following equation, which is related to local shear forces that are responsible for droplet break up [7].

$$\sigma_{w,p} = \frac{8\eta_c eJ\xi}{\varepsilon d_m}$$

where η_c is the continuous phase viscosity, J is the transmembrane flux, and ξ, ε, and d_m are the membrane tortuosity, porosity, and pore diameter, respectively. The relationship between the oil phase and emulsification results can be explained by the flow resistances and the disruption of droplets in pores of membrane. The extent of droplet disruption is related to the wall shear stress inside membrane pores.

In general, it is assumed that shear forces are responsible for droplet breakup during Premix MET. However, it is far from clear how these forces operate, and how they can be related to design of a process. One may expect that more mechanisms operate simultaneously [7]. For example, Van der Zwan et al. microscopically visualized the droplet breakup mechanism in O/W premix emulsification using microfluidic devices and found three factors responsible for breakup, that is the localized shear forces, the interfacial tension effects, and the steric hindrance between droplets [44].

(1) **Localized shear forces**
The breakup mechanism of premix membrane emulsification is due to the shear forces exerted on a droplet coming close to the tip of a channel branching, or due to divergent flow in both legs of a branching, e.g. *Y*- or *T*-shaped branching.

So, an expression for critical capillary number (C_{cr}) for breaking a droplet in the T junction can be utilized as follows [45]:

$$C_{cr} = \alpha\varepsilon_0\left(\frac{1}{\varepsilon_0^{2/3}} - 1\right)^2$$

where α is a dimensionless constant, which is a function of the viscosity contrast of the two fluids and the geometry of the channel. ε_0 is the droplet's initial extension before entering into the T junction, defined as the ratio of droplet length to its circumference.

(2) **Interfacial tension effects**

When a droplet is squeezed through the neck part in a membrane, the dumbbell-shape of the droplet gives rise to a difference in Laplace pressure between the dispersed phase inside the constraint (ΔP_c) and the dispersed phase before (ΔP_{d1}) and after (ΔP_{d2}) the neck part [45, 46]. So, the snap-off can take place when:

$$\left.\begin{aligned}\Delta P_c > \Delta P_{d1} \rightarrow \frac{\sigma}{R_{c1}} - \frac{\sigma}{R_{c2}} > \frac{2\sigma}{R_1}\\ \Delta P_c > \Delta P_{d2} \rightarrow \frac{\sigma}{R_{c1}} - \frac{\sigma}{R_{c2}} > \frac{2\sigma}{R_2}\end{aligned}\right\}$$

where R_{c1} and R_{c2} are the neck radii as shown in Figure 1.26. Further, R_1 and R_2 are the droplet radii before and after the neck part. If R_{c2} is much higher than R_{c1}, snap-off is induced when $2R_{c1} < R_1$ and $2R_{c2} < R_2$. Although shear forces may act simultaneously on the droplet, the lower value of critical capillary number (around 3×10^{-3}) in this case, indicates that the deformation of the droplet inside the neck part already destabilizes the droplets, along the lines of the interfacial tension-induced snap-off mechanism.

(3) **Steric hindrance between droplets**

The dispersed-phase droplets tend to accumulate inside the channels of the membrane. These accumulating droplets would experience collision with each other and thus induce breakup. Breakup in this case is strongly dependent on the interfacial properties. The stable emulsion will resist coalescence, and yield net steric breakup, while a less stable emulsion may coalesce [47].

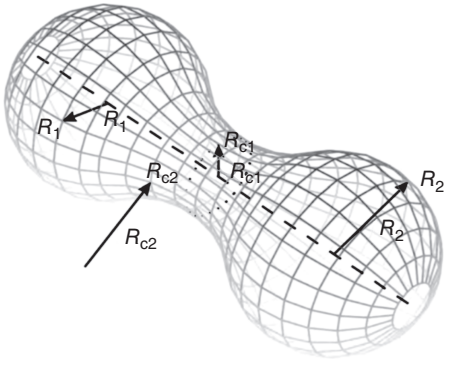

Figure 1.26 Schematic representation of the dumbbell-shaped droplet in a 3D constriction. Source: Link et al. [45]/with permission of Elsevier.

1.4 Summary

The birth of MET created a generation of platform for machinery manufacturing uniform emulsions and particles differing from the past thermodynamics method. It has been rousing great interest in recent decades for high throughput and facility to synthesize microspheres or microcapsules with a controlled size distribution (CV = 10–20%) at high productivity (several tons per hour). Precisely controlling process conditions with enough accuracy and achieving the maximum throughput for industrial production continuously become the general requirement for MET industrial applications. These optimizations and scaling up targeted for industry always rely on deep understanding of MET and decoding the relationship between emulsion droplets size and emulsification parameters, such as phase physical properties (viscosity, interfacial tension, etc.) and operation conditions (transmembrane pressure shear stress, continuous phase flow rate, etc.). Here, we systemically summarize the cognitions and development of principles and models in these years on two basic MET processes, the cross-flow MET and the premix MET. For cross-flow MET, the related mechanism has been thoroughly investigated not only experimentally but also theoretically, including the force and torque balance models, the CFD based models, Surface Evolver and Lattice Boltzmann-based models. Combining the microscope observations, they realize the prediction of both the droplet diameter and the uniformity of emulsion. Comparatively, the knowledge of premix MET is not as clear as cross-flow MET, especially on interaction mechanism between droplets and its influence on the final size of obtained droplets. Nevertheless, some processes that occur in cross-flow emulsification are also of relevance for premix emulsification design and process optimization. These cognitions make MET process more predictable and controllable, and thus provide significant guidance for operation optimization, recipe screening, and pilot scaling up of versatile emulsions.

References

1 Nakashima, T., Shimizu, M., and Kukizaki, M. (2000). Particle control of emulsion by membrane emulsification and its applications. *Advanced Drug Delivery Reviews* 45: 47–56.

2 Gijsbertsen Abrahamse, A.J., van der Padt, A., and Boom, R.M. (2004). Status of cross-flow membrane emulsification and outlook for industrial application. *Journal of Membrane Science* 230: 149–159.

3 Ma, G.H. (2014). Microencapsulation of protein drugs for drug delivery: strategy, preparation, and applications. *Journal of Controlled Release* 193: 324–340.

4 Song, C., Li, F., Wang, S. et al. (2019). Recent advances in particulate adjuvants for cancer vaccination. *Advances in Therapy* 3: 1900115.

5 Lambrich, U. and Schubert, H. (2005). Emulsification using microporous systems. *Journal of Membrane Science* 257: 76–84.

6 Schroder, V. and Schubert, H. (1999). Production of emulsions using microporous, ceramic membranes. *Colloids and Surfaces A: Physicochemical and Engineering Aspects* 152: 103–109.

7 Vladisavljevic, G.T., Shimizu, M., and Nakashima, T. (2004). Preparation of monodisperse multiple emulsions at high production rates by multi-stage premix membrane emulsification. *Journal of Membrane Science* 244: 97–106.

8 Vladisavljevic, G.T. and Schubert, H. (2002). Preparation and analysis of oil-in-water emulsions with a narrow droplet size distribution using Shirasu-porous-glass (SPG) membranes. *Desalination* 144: 167–172.

9 Gijsbertsen-Abrahamse, A.J., van der Padt, A., and Boom, R.M. (2003). Influence of membrane morphology on pore activation in membrane emulsification. *Journal of Membrane Science* 217: 141–150.

10 Vladisavljevic, G.T. and Schubert, H. (2003). Influence of process parameters on droplet size distribution in SPG membrane emulsification and stability of prepared emulsion droplets. *Journal of Membrane Science* 225: 15–23.

11 Luca, G.D., Sindona, A., Giorno, L., and Drioli, E. (2004). Quantitative analysis of coupling effects in cross-flow membrane emulsification. *Journal of Membrane Science* 229: 199–209.

12 Luca, G.D., Renzo, A.D., Maio, F.P.D., and Drioli, E. (2006). Modeling droplet formation in cross-flow membrane emulsification. *Desalination* 199: 177–179.

13 Hao, D.X., Gong, F.L., Hu, G.H. et al. (2008). Controlling factors on droplets uniformity in membrane emulsification: experiment and modeling analysis. *Industrial and Engineering Chemistry Research* 47: 6418–6425.

14 Rayner, M., Trägårdh, G., Trägårdh, C., and Dejmek, P. (2004). Using the surface evolver to model droplet formation processes in membrane emulsification. *Journal of Colloid and Interface Science* 279: 175–185.

15 Rayner, M., Trägårdh, G., and Trägårdh, C. (2005). The impact of mass transfer and interfacial expansion rate on droplet size in membrane emulsification processes. *Colloids and Surfaces A: Physicochemical and Engineering Aspects* 266: 1–17.

16 Kobayshi, I., Mukataka, S., and Nakajuma, M. (2004). CFD simulation and analysis of emulsion droplet formation from straight through microchannels. *Langmuir* 20: 9868–9877.

17 Van der Graaf, S., Nisisako, T., Schroen, C.G.P.H. et al. (2006). Lattice Boltzmann simulations of droplet formation in a T-shaped microchannel. *Langmuir* 22: 4144–4152.

18 Lian, G.P., Jousse, F., Janes, R., and Menech, M.D. (2007: Chapter 7). *Chemical Engineering Research Trends, Modelling the Formation and Flow of Multiphase Droplets in Microfluidics Devices*, 1–22. Nova Science Publishers Inc.

19 Yasuno, M., Nakajima, M., Iwamoto, S. et al. (2002). Visualization and characterization of SPG membrane emulsification. *Journal of Membrane Science* 210: 29–37.

20 Kobayashi, I., Nakajima, M., and Mukataka, S. (2003). Preparation characteristics of oil-in-water emulsions using differently charged surfactants in straight-through microchannel emulsification. *Colloids and Surfaces A: Physicochemical and Engineering Aspects* 229: 33–41.

21 Kobayashi, I. and Nakajima, M. (2002). Silicon array of elongated through-holes for monodisperse emulsion droplets. *AICHE Journal* 48: 1639–1644.

22 Sugiura, S., Nakajima, M., Iwamoto, S., and Seki, M. (2001). Interfacial tension driven monodispersed droplet formation from microfabricated channel array. *Langmuir* 17: 5562–5566.

23 Kobayashi, I., Mukataka, S., and Nakajima, M. (2005). Production of monodisperse oil-in-water emulsions using a large silicon straight-through microchannel plate. *Industrial and Engineering Chemistry Research* 44: 5852–5856.

24 De Luca, G., Maio, F.P.D., Renzo, A.D., and Drioli, E. (2008). Droplet detachment in cross-flow membrane emulsification: comparison among torque and force based models. *Chemical Engineering and Processing* 47: 1150–1158.

25 Wang, Z., Wang, S.C., Schroeder, V., and Schubert, H. (1999). Influence of fluid flow on forces acting on droplet and emulsification results in membrane emulsification process. *Chinese Journal of Chemical Engineering* 50: 505–513.

26 Peng, S.J. and Williams, R.A. (1998). Controlled production of emulsions using a crossflow membrane: part I: droplet formation from a single pore. *Chemical Engineering Research and Design* 76: 894–901.

27 Wang, Z., Wang, S., Schröder, V., and Schubert, H. (2000). Effect of continuous phase viscosity on membrane emulsification. *Chinese Journal of Chemical Engineering* 8: 108–112.

28 Schroder, V., Behrend, O., and Schubert, H. (1998). Effect of dynamic interfacial tension on the emulsification process using microporous ceramic membranes. *Journal of Colloid and Interface Science* 202: 334–340.

29 Xu, J.H., Luo, G.S., Chen, G.G., and Wang, J.D. (2005). Experimental and theoretical approaches on droplet formation from a micrometer screen hole. *Journal of Membrane Science* 266: 121–131.

30 De Luca, G. and Drioli, E. (2006). Force balance conditions for droplet formation in cross-flow membrane emulsifications. *Journal of Colloid and Interface Science* 294: 436–448.

31 Van der Graaf, S., Schroën, C.G.P.H., Van der Sman, R.G.M., and Boom, R.M. (2004). Influence of dynamic interfacial tension on droplet formation during membrane emulsification. *Journal of Colloid and Interface Science* 277: 456–463.

32 Yuyama, H., Watanabe, T., Ma, G.H. et al. (2000). Preparation and analysis of uniform emulsion droplets using SPG membrane emulsification technique. *Colloids and Surfaces A: Physicochemical and Engineering Aspects* 168: 159–174.

33 Abrahamse, A.J., Van der Padt, A., Boom, R.M., and de Heij, W.B.C. (2001). Process fundamentals of membrane emulsification: simulation with CFD. *AICHE Journal* 47: 1285–1291.

34 Abrahamse, A.J. (2003). *Membrane Emulsification: Process Principles*. Netherlands: Wagenningen University.

35 Christov, N.C., Ganchev, D.N., Vassileva, N.D. et al. (2002). Capillary mechanisms in membrane emulsification: oil-in-water emulsions stabilized by Tween 20 and milk proteins. *Colloids and Surfaces A: Physicochemical and Engineering Aspects* 209: 83–104.

36 Kobayashi, I. and Nakajima, M. (2002). Effect of emulsifiers on the preparation of food-grade oil-in-water emulsions using a straight-through extrusion filter. *European Journal of Lipid Science and Technology* 104: 720–727.

37 Timgren, A., Tragardh, G., and Tragardh, C. (2009). Effects of pore spacing on drop size during cross-flow membrane emulsification—A numerical study. *Journal of Membrane Science* 337: 232–239.

38 Lepercq Bost, E., Giorgi, M., Isambert, A., and Arnaud, C. (2010). Estimating the risk of coalescence in membrane emulsification. *Journal of Membrane Science* 357: 36–46.

39 Egidi, E., Gasparini, G., Holdich, R.G. et al. (2008). Membrane emulsification using membranes of regular pore spacing: droplet size and uniformity in the presence of surface shear. *Journal of Membrane Science* 323: 414–420.

40 Kosvintsev, S.R., Gasparini, G., and Holdich, R.G. (2008). Membrane emulsification: droplet size and uniformity in the absence of surface shear. *Journal of Membrane Science* 313: 182–189.

41 Lepercq-Bost, E., Giorgi, M., Isambert, A., and Arnaud, C. (2008). Use of capillary number for the prediction of droplet size in membrane emulsification. *Journal of Membrane Science* 314: 76–89.

42 Pathak, M. (2011). Numerical simulation of membrane emulsification: effect of flow properties in the transition from dripping to jetting. *Journal of Membrane Science* 382: 166–176.

43 Sugiura, S., Nakajima, M., Kumazawa, N. et al. (2002). Characterization of spontaneous transformation-based droplet formation during microchannel emulsification. *The Journal of Physical Chemistry* 106: 9405–9409.

44 Zwan, E.V.D., Schroën, K., Dijke, K.V., and Boom, R. (2006). Visualization of droplet break-up in pre-mix membrane emulsification using microfluidic devices. *Colloids and Surfaces A: Physicochemical and Engineering Aspects* 277: 223–229.

45 Link, D.R., Anna, S.L., Weitz, D.A., and Stone, H.A. (2004). Geometrically mediated breakup of drops in microfluidic devices. *Physical Review Letters* 92: 054503.

46 Roof, J.G. (1970). Snap-off of oil droplets in water-wet pores. *Society of Petroleum Engineers Journal* 10: 85–90.

47 Nazir, A., Schroën, K., and Boom, R. (2010). Premix emulsification: a review. *Journal of Membrane Science* 362: 1–11.